Ratcheting and fatigue behavior of Eurofer97 at high temperature, part 2: modeling

Kuo Zhang[1,2], Jarir Aktaa[1]

[1]Karlsruhe Institute of Technology, Institute for Applied Materials, Hermann-von-Helmholtz-Platz 1, 76344 Eggenstein-Leopoldshafen, Germany

[2]Max Planck Institute of Plasma Physics, Boltzmannstraße 2, 85748 Garching, Germany

Abstract

A constitutive model is proposed for Reduced-Activation Ferritic-Martensitic (RAFM) steel Eurofer97 at high temperatures by combining formulae from previous modeling approaches to describe and predict mechanical behaviors under various cyclic loading conditions. Two failure modes, fatigue fracture and over-accumulated strain (ratcheting) are able to be simulated by the combined constitutive model. Cyclic softening and the effect of magnitude, symmetry and rate of external loading on ratcheting behavior are also able to be described by the new model. Parameter values are fitted based on strain-controlled and stress-controlled isothermal uniaxial experiments on Eurofer97 batch two at 450°C and 550°C. The simulated results are presented to compare with corresponding experimental data, to show the performance of the new constitutive model.

Key words

Eurofer97; constitutive model; 450°C and 550°C

1. Introduction

Eurofer97 is considered as one of the candidates of structural materials for first wall and blanket systems of future fusion power plant [1-3]. Due to frequent startups, shutdowns and load fluctuations, the components in fusion power plant are under complex cyclic thermo-mechanical loadings which can lead to different mechanical damages.

In part 1, mechanical behaviors including cyclic softening, fatigue crack and ratcheting of Eurofer97 have been evaluated. Since these phenomena will appear simultaneously under complex cyclic loading, they shall be all considered in the design of construction rules for the structural materials in reactor.

According to experiments presented in part 1, cyclic softening and fatigue crack appear in strain-controlled low cycle fatigue (LCF) tests, and ratcheting appears in stress-controlled cyclic tests. A constitutive model is expected, which is able to simulate and predict mechanical behaviors in both strain- and stress-controlled cyclic loadings.

In the previous researches, a constitutive model has been proposed to describe the ratcheting behavior of mod. 9Cr-1Mo ferritic martensitic (FM) steel P91 [4]. Comparing to other modeling approaches for ratcheting [5-11], the model presented in [4] follows the Aktaa-Schmitt model [2], a modification of the Chaboche model [12]. This model in [4] has inherited from Aktaa-Schmitt model the equations for describing visco-plasticity, and the Armstrong-Frederick equation [13] for kinematic hardening.

The difference is that, the model in [4] has reduced the number of back stress (BS) components from four, eight and even 12 in [5-11] to only two. And conversely, this model has increased the number of BS from only one in Aktaa-Schmitt model [2] to two, since one BS component described by Armstrong-Frederick equation leads to overestimation of ratcheting. Note that in the theory of solid mechanics concerning flow laws, back stress is referred to as “kinematic hardening variable”. It is also known as the “microstress component” [13]. More back stress components add together to describe the kinematic hardening.

Although generally a model with more parameters can be more precise to describe and predict the real world, it increases the efforts to find the correct parameters. It has been found that two BS components are enough to describe the ratcheting behavior: both follow the Armstrong-Frederick model, one is to describe the stress-strain hysteresis loops, another one is to match the accumulated strains in ratcheting.

On the other hand, to describe and predict the fatigue crack under cyclic loading, a damage variable is required in the constitutive model. In the previous study on the deformation and damage behavior of Eurofer97 batch one under LCF loading [2], a damage variable has been proposed.

Note that however, in the previous modeling for P91 [4], the damage variable is eliminated since no macro fatigue fracture has appeared on any ratcheting specimens. And an initial modeling for Eurofer97 at 550°C has been reported in [14], however also without damage variable. Comparing to the modeling approach reported in [4] and [14], the damage variable is included in the current work, and the parameter values for Eurofer97 at 550°C have been further fitted for better modeling performance.

2. Requirements in modeling

Based on the experimental results reported in part 1, a database including strain-controlled LCF tests and stress-controlled ratcheting tests for Eurofer97 batch two at both 450°C and 550°C is

built. To analyze the mechanical behavior and predict material responses under more arbitrary loading conditions, a model was built to simulate the mechanical behavior of Eurofer97.

The model description should agree with material responses qualitatively and quantitatively. According to experimental results, the simulated results should fulfill the following criteria:

1. Fitting on accumulated strain under multiple loading conditions.
2. Fitting on fatigue lifetimes in strain-controlled LCF tests.
3. Showing cyclic softening in strain-controlled LCF tests.
4. Higher peak stress leads to higher ratcheting rate.
5. Highest ratcheting rate with stress ratio between -1 and -0.9.
6. Higher ratcheting rate with lower stress rate and vice versa.

Since the over-accumulated strain in ratcheting and the fatigue fracture are considered as failure modes, the first two criteria are the most important ones.

3. Modeling

Firstly the total strain is combined by elastic and inelastic strains:

$$\boldsymbol{\varepsilon}=\boldsymbol{\varepsilon}^{el}+\boldsymbol{\varepsilon}^{in} \qquad \text{eq. 1}$$

The elastic strain follows the Hooke's law for isotropic materials:

$$\boldsymbol{\varepsilon}^{el}=\frac{(1+\upsilon)}{E}\tilde{\boldsymbol{\sigma}}-\frac{\upsilon}{E}(trace(\tilde{\boldsymbol{\sigma}}))\mathbf{1} \qquad \text{eq. 2}$$

$$\tilde{\boldsymbol{\sigma}}=\frac{\boldsymbol{\sigma}}{1-D} \qquad \text{eq. 3}$$

$\tilde{\boldsymbol{\sigma}}$ is the effective stress tensor due to damage D. The damage factor is supposed to describe the total effect of porosities including e.g. fatigue induced micro- and macro crack. The effective cross section of the specimen is $\tilde{A}=A(1-D)$. In the extreme situation, the as received specimen has D = 0 and the totally broken specimen has D = 1. Hence, the effective stress $\tilde{\boldsymbol{\sigma}}$ is as in eq. 3. E is Young's modulus and υ is Poisson's ratio.

The development of inelastic strain $\dot{\boldsymbol{\varepsilon}}^{in}$ follows the Aktaa-Schmitt model[2], as shown in eq. 4. K, Z and n are material and temperature dependent parameters. Z and n control the visco-plasticity of the material. $\boldsymbol{\Omega_1}$ and $\boldsymbol{\Omega_2}$ are two tensor variables as BS components to describe the kinematic hardening. K defines the magnitude of the initial elastic regime, under which, there is absolutely no inelastic deformation. The cyclic softening is expressed by a scalar variable ψ which is introduced in the flow rule (eq. 4) in a way allowing the consideration of the impact of cyclic softening on all parts of the stress among others the kinematic hardening. Note that in other modeling approach such as [15] for mod. 9Cr-1Mo FM steel, the cyclic softening is

expressed by a decreasing magnitude of the elastic regime K. However, based on the discussion in [2], the cyclic softening not only reduces the elastic regime, but also the capacity for kinematic hardening as well as its viscosity.

$$\dot{\boldsymbol{\varepsilon}}^{in} = \frac{3}{2}\left\langle\frac{\Sigma_{eq}-K}{Z}\right\rangle^{n}\frac{\boldsymbol{\Sigma}}{\Sigma_{eq}} \qquad \text{eq. 4}$$

with $\boldsymbol{\Sigma} = \frac{\tilde{\boldsymbol{s}}}{\psi} - \boldsymbol{\Omega_1} - \boldsymbol{\Omega_2}$, $\tilde{\boldsymbol{s}} = \tilde{\boldsymbol{\sigma}} - \frac{1}{3}trace(\tilde{\boldsymbol{\sigma}})\mathbf{1}$ *and* $\Sigma_{eq} = \sqrt{\frac{3}{2}\boldsymbol{\Sigma}:\boldsymbol{\Sigma}}$

ψ is a combination of ψ_1 and ψ_2. ψ_1 describes the softening rate during the second cyclic softening stage. ψ_2 describes the softening rate during the initial rapid softening. h, c , c_s and ψ_s are material and temperature dependent parameters.

$$\psi = \psi_1 + \psi_2 \qquad \text{eq. 5}$$
$$with\ \psi_1(t=0) = 0\,,\ \psi_2(t=0) = 1$$

$$\dot{\psi}_1 = -h\dot{p}$$
$$\dot{\psi}_2 = c(\psi_s - \psi_2)\dot{p} - r_\psi|\psi_2 - \psi_r|^{m_\psi - 1}(\psi_2 - \psi_r)$$
$$with\ \psi_s = 1 - \psi_{s,\infty}(1 - \exp(-c_s \max_{-\infty<\tau<t}\left|\varepsilon^{in}(\tau)\right|))$$

$\dot{p}$ is the rate of the accumulated inelastic deformation and is determined by the tensor of inelastic strain $\dot{\boldsymbol{\varepsilon}}^{in}$ as

$$\dot{p} = \sqrt{\frac{2}{3}\dot{\boldsymbol{\varepsilon}}^{in}:\dot{\boldsymbol{\varepsilon}}^{in}} \qquad \text{eq. 6}$$

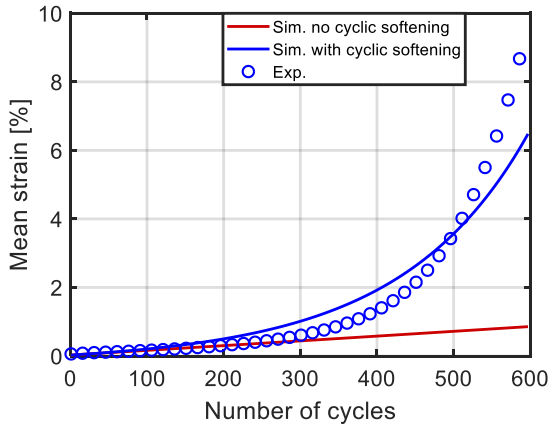

Figure 1 Comparison between simulation with and without cyclic softening, with stress alternating between 380 and -342Mpa

The inclusion of the cyclic softening variable is crucial in the modeling for ratcheting. As shown in

Figure 1, if the softening variable is eliminated from the constitutive model, the simulated result (red curve) underestimates the accumulated strain.

The equation for the damage variable follows the equation in the previous study[2]:

$$\dot{D} = \langle \frac{\chi(\boldsymbol{\sigma})}{A} \rangle^r \dot{p} \ (1-D)^{-\kappa} \qquad \text{eq. 7}$$

$\chi(\boldsymbol{\sigma})$ is simplified to be $\sqrt{\frac{3}{2}\boldsymbol{s}:\boldsymbol{s}}$ with $\boldsymbol{s} = \boldsymbol{\sigma} - \frac{1}{3}Trace(\boldsymbol{\sigma})\mathbf{1}$.

Part 1 of the current work has discussed the reason, why there is no fatigue fracture on any specimens in ratcheting tests. The inelastic strain ranges during two tests have been compared: one for the strain-controlled LCF test with total strain range 1%, the other one for the stress-controlled ratcheting test with stress alternating between 380 and -342MPa. It has been found that the inelastic strain in the strain-controlled test is much larger than that in the stress-controlled test. Also, the initial stress range in this strain-controlled test is around 900MPa, which is larger than the constant stress range 380+ 342 = 722MPa. According to eq. 7, the damage accumulates much earlier in this strain-controlled test. Besides, damage also accelerates the increase of itself. Hence the initial larger inelastic strain and larger stress lead to larger damage and earlier fatigue fracture in the strain-controlled LCF tests.

The equations of the two BS components are:

$$\dot{\boldsymbol{\Omega}}_{\mathbf{1}} = \frac{2}{3}H_1\dot{\boldsymbol{\varepsilon}}^{in} - C_1\boldsymbol{\Omega}_1\dot{p} - R_1J(\boldsymbol{\Omega}_1)^{m_1-1}\boldsymbol{\Omega}_1$$

$$\textit{with } J(\boldsymbol{\Omega}_1) = \sqrt{\frac{3}{2}\boldsymbol{\Omega}_1:\boldsymbol{\Omega}_1} \qquad \text{eq. 8}$$

$$\dot{\boldsymbol{\Omega}}_{\mathbf{2}} = \frac{2}{3}H_2\dot{\boldsymbol{\varepsilon}}^{in} - J(\boldsymbol{\Omega}_2)^{n_2-1}\boldsymbol{\Omega}_2\,\langle\dot{\boldsymbol{\varepsilon}}^{in}:\frac{\boldsymbol{\Omega}_2}{r_2}\rangle - R_2J(\boldsymbol{\Omega}_2)^{m_2-1}\boldsymbol{\Omega}_2$$

$$\textit{with } J(\boldsymbol{\Omega}_2) = \sqrt{\frac{3}{2}\boldsymbol{\Omega}_2:\boldsymbol{\Omega}_2} \qquad \text{eq. 9}$$

The equation for BS component 1 ($\boldsymbol{\Omega}_1$) follows the conventional Armstrong-Frederick model [13] with $C_1\boldsymbol{\Omega}_1\dot{p}$ as dynamic recovery of kinematic hardening and $R_1J(\boldsymbol{\Omega}_1)^{m_1-1}\boldsymbol{\Omega}_1$ as static recovery of kinematic hardening.

The equation for BS component 2 ($\boldsymbol{\Omega}_2$) originates from the Armstrong-Frederick model, as similar to other modeling approaches for ratcheting [5, 7, 11]. However, the current equation for $\boldsymbol{\Omega}_2$ includes a specially chosen term for the dynamic recovery of $\boldsymbol{\Omega}_2$, so that no more than two BS components are required to describe the ratcheting behavior.

As well known in the modeling for ratcheting [5-11], with only one BS component following Armstrong-Frederick, the model will overestimate the ratcheting. In the current modeling approach, BS 2 is included to minimize the effect of mean stress of the external loading. As an

example, shown in Figure 2 a), the mean value of BS1 and BS2, as well as their summation in each loading cycle are shown, for the case of peak stress 380MPa and stress ratio -0.9.

The mean stress of the external loading is 19MPa. With the carefully designed equation of BS2, the mean value of BS2 is close to 19MPa. Hence the effect of asymmetric external loading is largely reduced. The effect is much clearer if cyclic softening is not included in simulation, as shown in Figure 2 b). The sum of mean values of BS1 &2 is kept at 18.8MPa after around 10 initial cycles, which is very close to 19MPa as the external mean stress.

On the other hand, it is demonstrated that, with this equation for BS2 (eq. 9), the model is already able to match the accumulated strains in various experimental ratcheting results. Therefore no additional BS components are necessary.

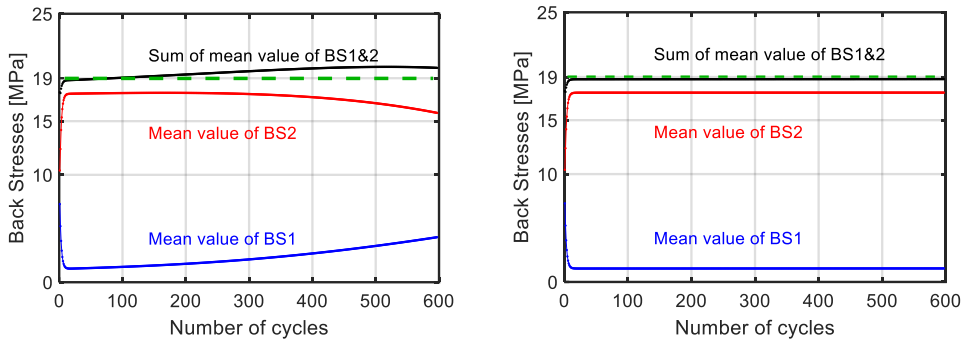

Figure 2 Simulated mean values of BS 1&2 in each loading cycle, with stress alternating between 380 and -342MPa. a) with cyclic softening variable. b) without cyclic softening variable.

While choosing the equation for $\boldsymbol{\Omega}_2$, several alternatives for the dynamic recovery part have been tested in simulation:

$$J(\boldsymbol{\Omega}_2)^{n_2-1}\boldsymbol{\Omega}_2\langle\dot{p}\rangle\left\langle\frac{\boldsymbol{\Omega}_2}{r_2}\right\rangle \qquad \text{eq. 10}$$

$$J(\boldsymbol{\Omega}_2)^{n_2-1}\boldsymbol{\Omega}_2|\dot{p}|\left\langle\frac{\boldsymbol{\Omega}_2}{r_2}\right\rangle \qquad \text{eq. 11}$$

$$|J(\boldsymbol{\Omega}_2)^{n_2-1}\dot{p}|\boldsymbol{\Omega}_2\left\langle\frac{\boldsymbol{\Omega}_2}{r_2}\right\rangle \qquad \text{eq. 12}$$

$$\langle J(\boldsymbol{\Omega}_2)^{n_2-1}\dot{p}\rangle\boldsymbol{\Omega}_2\left\langle\frac{\boldsymbol{\Omega}_2}{r_2}\right\rangle \qquad \text{eq. 13}$$

$$J(\boldsymbol{\Omega}_2)^{n_2-1}\boldsymbol{\Omega}_2\left|\dot{\boldsymbol{\varepsilon}}^{in}:\frac{\boldsymbol{\Omega}_2}{r_2}\right| \qquad \text{eq. 14}$$

It is found that eq. 10 to eq. 13 do not yield negative accumulated strain when the mean stress is negative.

However, the difference between simulated results by applying eq. 9 and eq. 14 is marginal. The difference lay on the Macaulay bracket $\langle x\rangle = \frac{x+|x|}{2}$ and the absolute value $|x|$. The Macaulay

bracket is more reasonable based on the hypothesis that the dynamic recovery is supposed to occur only when BS and inelastic strain rate having the same direction. This hypothesis follows the modeling approach of the Ohno-Wang model [6]. However, according to the Armstrong-Frederick model [13], dynamic recovery also occurs when BS and inelastic strain rate have opposite directions. The physical background was not discussed in Ohno and Wang's reports [5, 6], or in Armstrong and Frederick's report [13]. Ohno and Abdel–Karim [7] simply combined ideas from [5, 6, 13] into eq. 15 without further discussion from the physical point of view.

$$\dot{\boldsymbol{\Omega}}_i = \frac{2}{3} H_i \dot{\boldsymbol{\varepsilon}}^{in} - \mu_i C_i \boldsymbol{\Omega}_i \dot{p} - Hs(f_i) C_i \langle \dot{\lambda}_i \rangle \boldsymbol{\Omega}_i \qquad \text{eq. 15}$$

With $\dot{\lambda}_i = \dot{\boldsymbol{\varepsilon}}^{in} : \frac{\boldsymbol{\Omega}_i}{r_i} - \mu_i \dot{p}$, $f_i = \overline{\boldsymbol{\Omega}}_i^{\,2} - r_i^{\,2}$

Hs in eq. 15 denotes the Heaviside step function, which operates as $Hs(x) = 0$ when $x < 0$ and $Hs(x) = 1$ when $x \geq 0$.

The section in which the BS and inelastic strain rate having opposite signs is illustrated in red in the stress–strain hysteresis loop shown in Figure 3. In spite of the difference from the physical point of view, the simulated results are similar when using the Macaulay bracket (eq. 9) and the absolute value (eq. 14). Figure 4 illustrates the comparison of increasing rate of BS 2 between application of the Macaulay bracket (blue curve) and the absolute value (red curve). As can be seen, the blue and red curves coincide with each other, except for two short sections, and the deviation is relatively small. Hence, the simulated results are similar.

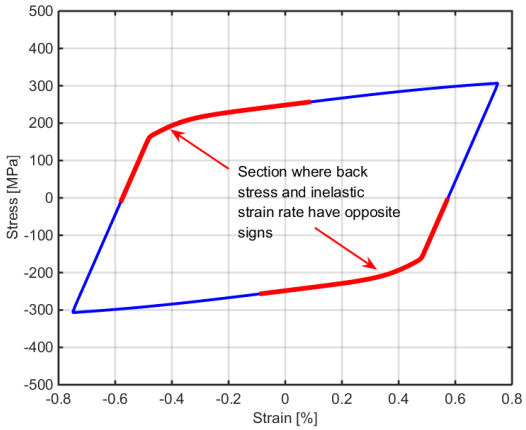

Figure 3 Simulated stress–strain hysteresis loop of 200th cycle in the strain-controlled LCF test performed with $\Delta\varepsilon$ = 1.5% at 550 °C

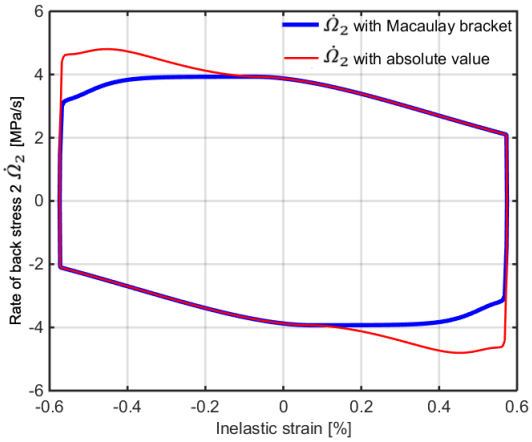

Figure 4 Comparison between applying Macaulay bracket and absolute value, simulated result: 200th cycle of the strain-controlled LCF test performed with $\Delta\varepsilon$ = 1.5% at 550 °C, increasing rate of BS 2 vs. inelastic strain

In the current study, only uniaxial LCF and ratcheting tests are performed. Hence the multiaxial form of the constitutive model is transformed to a uniaxial form.

The stress tensor under uniaxial loading is

$$\boldsymbol{\sigma} = \sigma \begin{pmatrix} 1 & & \\ & 0 & \\ & & 0 \end{pmatrix} \qquad \text{eq. 16}$$

Hence the following uniaxial formulation is obtained:

$\dot{\varepsilon} = \dot{\varepsilon}^{in} + \dot{\varepsilon}^{el}$	*eq. 17*
$\varepsilon^{el} = \frac{\sigma}{E(1-D)}$	eq. 18
$\dot{D} = \langle\frac{\sigma}{A}\rangle^{r} \lvert\dot{\varepsilon}^{in}\rvert \ (1-D)^{-\kappa}$	eq. 19
$\dot{\varepsilon}^{in} = \langle\frac{\lvert\Sigma\rvert - K}{Z}\rangle^{n} sgn(\Sigma) \ \ with\ \Sigma = \frac{\sigma}{\psi(1-D)} - \Omega_1 - \Omega_2$	eq. 20
$\psi = \psi_1 + \psi_2, with\ \psi_1(t=0) = 0\ and\ \psi_2(t=0) = 1$	eq. 21
$\dot{\psi}_1 = -h\lvert\dot{\varepsilon}^{in}\rvert$	eq. 22
$\dot{\psi}_2 = c\left(1 - \psi_{s,\infty} - \psi_2\right)\left\lvert\dot{\varepsilon}^{in}\right\rvert - r_{\psi}\lvert\psi_2 - \psi_r\rvert^{m_{\psi}-1}(\psi_2 - \psi_r)$	eq. 23
$\dot{\Omega}_1 = H_1\dot{\varepsilon}^{in} - C_1\Omega_1\left\lvert\dot{\varepsilon}^{in}\right\rvert - R_1\lvert\Omega_1\rvert^{m_1-1}\Omega_1$	eq. 24
$\dot{\Omega}_2 = H_2\dot{\varepsilon}^{in} - \lvert\Omega_2\rvert^{n_2-1}\Omega_2\,\langle\dot{\varepsilon}^{in}\frac{\Omega_2}{r_2}\rangle - R_2\lvert\Omega_2\rvert^{m_2-1}\Omega_2$	eq. 25

Table 1 Equations of the constitutive model in uniaxial form

Comparing to multiaxial form, $\dot{p}$ is written as $\left\lvert\dot{\varepsilon}^{in}\right\rvert$. The strain tensor under uniaxial loading is

$$\dot{\boldsymbol{\varepsilon}}^{in} = \dot{\varepsilon}^{in}\begin{pmatrix} 1 & & \\ & -\frac{1}{2} & \\ & & -\frac{1}{2} \end{pmatrix} \qquad \text{eq. 26}$$

The tensors of the two back stress components are

$$\dot{\boldsymbol{\Omega}}_{\mathbf{1,2}} = \dot{\Omega}_{1,2}\begin{pmatrix} \frac{2}{3} & & \\ & -\frac{1}{3} & \\ & & -\frac{1}{3} \end{pmatrix} \qquad \text{eq. 27}$$

4. Modeling results

The parameters (E, K, Z, n, h, c, r_{ψ}, ψ_r, m_{ψ}, $\psi_{s,\infty}$, c_s H_1, C_1, R_1, m_1, H_2, r_2, R_2, m_2, n_2, A, r, κ) are fitted using a program named MINUIT developed at CERN which uses variable-metric method with inexact line search to find the minimum of functions [16].

Detailed fitting steps are similar to the ones presented in the previous work [2] which focuses on the cyclic softening and fatigue fracture of Eurofer97 batch 1 as well as steel F82H

mod. The concept of the fitting steps is initially to fit several parameters with some relevant experimental data, for instance ratcheting data for fitting H_2, r_2, R_2, m_2, n_2; and data of low cycle fatigue lives for fitting A, r, κ. After one group of parameters is fitted, these values are fixed and the next group will be fitted. In the end, all parameters are fitted with all experimental data, to find a compromise between various parameter values.

It is found that some alternatives of parameter values also lead to less satisfying however acceptable simulation results. The current fitting result is limited to the current available experimental data. The parameter values can be modified after more experiments performed in the future, under more loading conditions.

On the other hand, one of the achievements in the current modeling approach is reducing the number of parameters, by reducing the number of back stress components from four, eight or even 12 [5-11] to only two. Each back stress component includes at least two parameters in the constitutive model.

The fitted parameter values for Eurofer97 batch two are listed in Table 2.

	Eurofer97 550°C	Eurofer97 450°C
$E\ (MPa)$	165800	186700
$K\ (MPa)$	24.562	219.34
$Z\ (MPa\ s^{1/n})$	364.67	177.31
n	24	20.608
$H_1\ (MPa)$	198980	96255
C_1	1959.8	1683.1
$R_1(MPa^{1-m_1}s^{-1})$	6.45×10^{-12}	1.964×10^{-7}
m_1	4.5984	2.6797
$H_2\ (MPa)$	25700	88643
r_2	23.855	0.8447
$R_2(MPa^{1-m_2}s^{-1})$	1×10^{-12}	0
m_2	9.536×10^{-6}	/
n_2	6.596	/
h	1.6×10^{-3}	8×10^{-3}
c	2.5	1.6445
$r_\psi\ (s^{-1})$	3.27×10^{-4}	2.624×10^{-6}
ψ_r	0.99	0.830
m_ψ	0.9636	1.0563
$\psi_{s,\infty}$	0.4233	0.20239
c_s	1200	2000
A	3233.9	1866.3
r	2.0818	3.0615
κ	18.98	43.16

Table 2 Fitted parameter values for Eurofer97-2 at 450°C and 550°C

The fitted value of R_2 for 450°C is negligible. Hence the static recovery of BS2 is set to zero.

Due to the complexity of the constitutive model, it is possible that various combinations of parameter values generate similar simulated results. Since, except the Young's modulus, all other parameters cannot be directly measured with physical method, the possibility exists, that the parameter values would be further optimized, or even the formulation of the constitutive model would be modified with more available experimental data of the material.

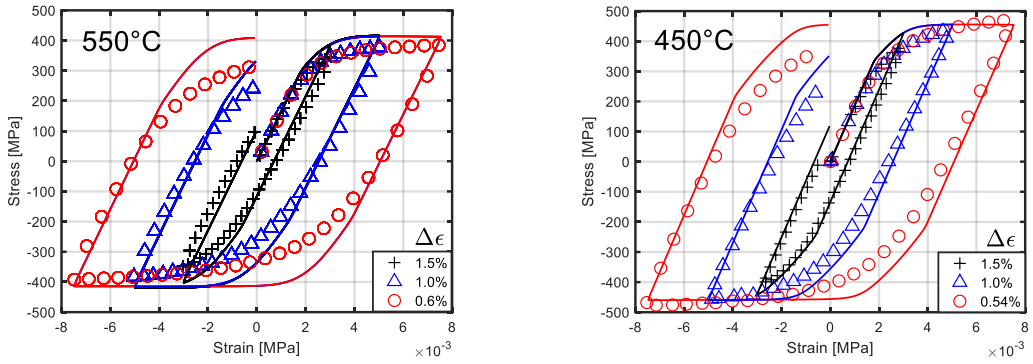

a) b)

Figure 5 Hysteresis loops of the first loading cycle with various total strain ranges. a) 550°C b) 450° C.

Figure 5 shows the comparison between the simulated hysteresis loops (curves) and the experimental data (markers), with various total strain ranges in strain-controlled LCF tests.

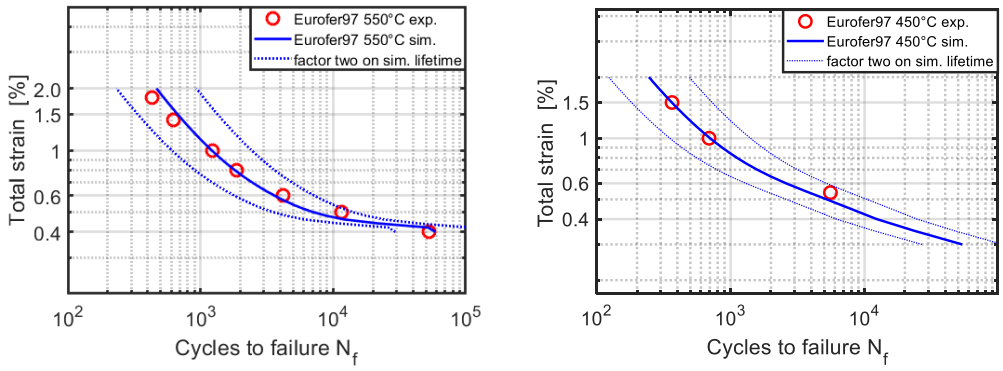

a) b)

Figure 6 Relationships of total strain ranges vs. number of cycles to failure. a) 550°C b) 450° C.

Figure 6 shows the simulated curves of total strain ranges vs. number of cycles to failure (lifetime), with experimental data for comparison. Dashed curves are drawn to illustrate the half and twice of the simulated lifetime, namely “factor two”. The experimental data points located within the factor two ranges, both for 450°C and 550°C. Hence the simulation performance of the model is satisfying in terms of lifetime prediction.

Despite the lack of experimental data, the currently available data have already covered most of the range of total strain in the usual evaluation of low cycle fatigue. For a comprehensive data base of Eurofer97 batch 2, more fatigue tests shall be performed at various testing temperatures. Such testing campaign will be done in the future by various laboratories in European Union as for batch 1 material [17, 18].

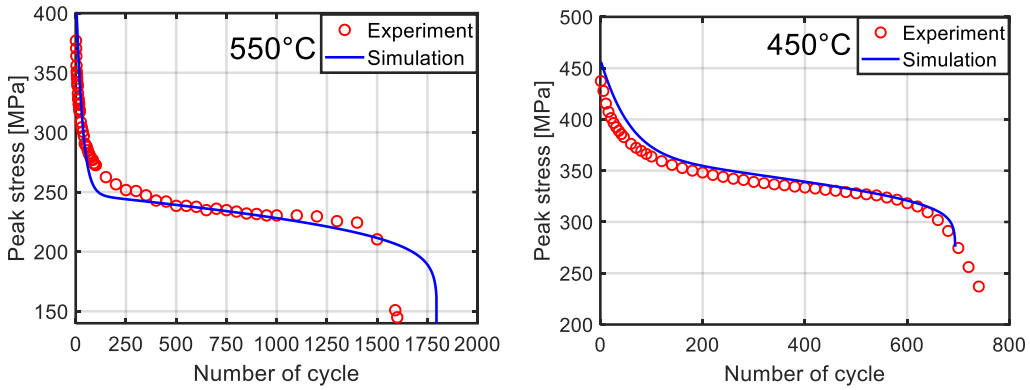

a) b)

Figure 7 Peak stress in each loading cycle, with total strain range 1%. a) 550°C b) 450° C.

Figure 7 shows the simulated and experimental results of peak stresses in each loading cycle in the strain-controlled LCF tests with total strain range 1%, and with one example for each testing temperature. Both simulated and experimental results show rapid decrease of peak stresses in the initial loading cycles and a saturated decrease afterwards, followed by again rapid decrease of the peak stress. The rapid decrease of the peak stresses near the end of lifetime is due to damage variable D, which describes the effect of fatigue crack growth in the experiments. It is obvious that the model is able to describe the cyclic softening of the material.

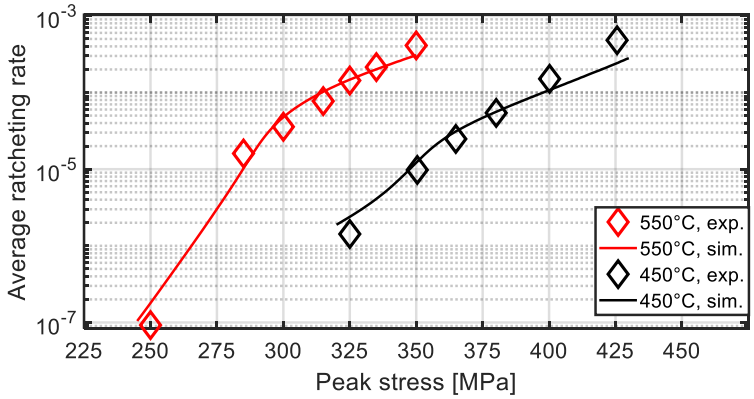

Figure 8 Average ratcheting rates vs. peak stresses in ratcheting tests.

Figure 8 shows the relationship between the average ratcheting rate and the peak stresses in stress-controlled ratcheting tests. At 550°C, the peak stresses range from 250MPa to 350MPa. At 450°C, the peak stresses range from 325MPa to 425MPa. The stress ratios are kept at -0.9. The simulated curves match well with the experimental data points. Hence, the model satisfies the criterion “higher peak stress leads to higher ratcheting rate.”

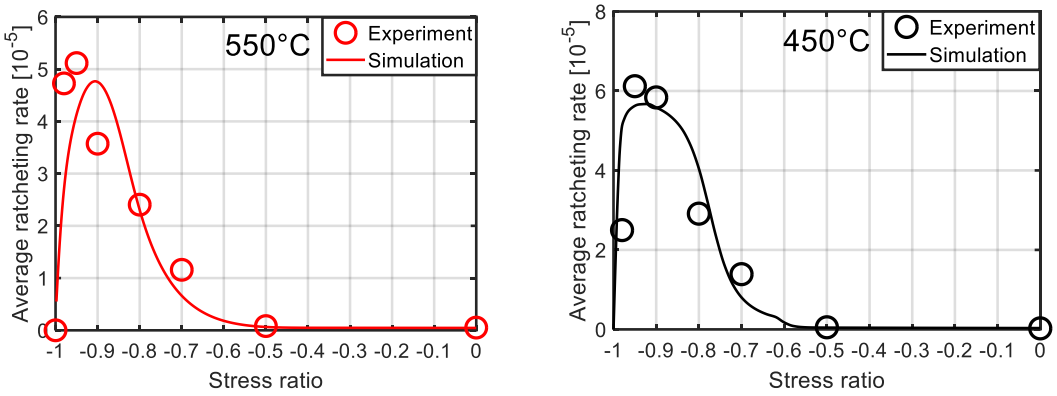

a) b)

Figure 9 Average ratcheting rates vs. stress ratios in ratcheting tests. a) 550°C b) 450° C.

Figure 9 shows the relationship between the average ratcheting rates and the stress ratios in stress-controlled ratcheting tests. The stress ratios range from -1 to 0, which means that the loading change from symmetric loading to monotonic tensile loading. At 550°C, the peak stresses are kept at 300MPa. At 450°C, the peak stresses are kept at 380MPa. Both simulated and experimental results show hill-like relationship, with its peak between stress ratio -1 and -0.9. The ratcheting behavior is relatively negligible when stress ratio is between -0.5 and zero, due to lack of inelastic deformation. Detailed discussion of such hill-like relationship shown in Figure 9 can be found in part 1.

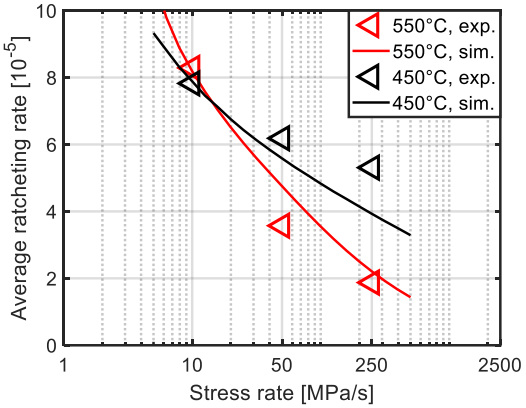

Figure 10 Average ratcheting rates vs. stress rates in ratcheting tests.

Figure 10 shows the relationship between the average ratcheting rate and the stress rates for both 550°C and 450°C. The stress rates in experiments are 10, 50 and 250MPa/s. At 550°C, the peak stresses are 300MPa, stress ratios are -0.9. At 450°C, the peak stresses are 380MPa, stress ratios are -0.9. Obviously, higher stress rates lead to slower ratcheting, both in experimental and simulated results. Further, the influence of stress rate is larger at 550°C than at 450°C, which indicates higher visco-plasticity at higher temperature.

Generally speaking, a comprehensive constitutive model should be able to predict mechanical and failure behavior under as many loading conditions as possible. However modeling is usually

limited to describe some certain type of mechanical behavior. As the second part of the work, which focuses on the modeling approach, the purpose is to build a constitutive model to describe the experiments presented in part 1. Part 1 focuses on the physical background of the uniaxial and isothermal cyclic behavior of Eurofer97 at 450°C and 550°C, including the strain-controlled low cycle fatigue and stress-controlled ratcheting. In the future, more experiments, e.g. multi-axial ratcheting tests, will be planned in order to validate the prediction ability of the proposed model in the current work.

The long term purpose of the research is to build a model for finite element method to predict the life time of components in nuclear power plants with working temperatures between 450°C and 550°C.

5. Conclusions

The new proposed constitutive model has combined damage variable, softening variable and with two back stress components. The simulation performance of this model is demonstrated to be satisfying, since fatigue fracture, over-accumulated strain as two failure modes have been described. The new model continues to be able to describe cyclic softening. Further, the new model also describes the effects of three influencing factors on ratcheting behavior:

1. higher peak stress leads to faster ratcheting.
2. highest ratcheting rate with stress ratio between -1 and -0.9.
3. higher ratcheting rate with lower stress rate and vice versa.

Parameter values have been fitted based on experimental data of Eurofer97 batch two at two testing temperatures: 450°C and 550°C. The simulated results matches fairly well with the material's mechanical behavior. Further mechanical tests at other temperatures are expected aiming a constitutive model which is able to describe and predict the mechanical behavior under arbitrary loading conditions.

Acknowledgement

This work is carried out within the R&D Nuclear Fusion Program of the Karlsruhe Institute of Technology (KIT).

Reference

[1] B. Raj and T. Jayakumar, "Development of Reduced Activation Ferritic–Martensitic Steels and fabrication technologies for Indian test blanket module", *Journal of Nuclear Materials,* vol. 417, pp. 72-76, 2011.

[2] J. Aktaa and R. Schmitt, "High temperature deformation and damage behavior of RAFM steels under low cycle fatigue loading: Experiments and modeling", *Fusion Engineering and Design,* vol. 81, pp. 2221-2231, 2006.

[3] V. B. Oliveira, H. R. Z. Sandim, and D. Raabe, "Abnormal grain growth in Eurofer-97 steel in the ferrite phase field", *Journal of Nuclear Materials,* vol. 485, pp. 23-38, 2017.

[4] K. Zhang and J. Aktaa, "Characterization and modeling of the ratcheting behavior of the ferritic–martensitic steel P91", *Journal of Nuclear Materials,* vol. 472, pp. 227-239, 2016.

[5] N. Ohno and J. D. Wang, "Kinematic Hardening Rules with Critical State of Dynamic Recovery, Part I: Formulation and basic features for ratchetting behavior", *International Journal of Plasticity,* vol. 9, pp. 375-390, 1993.

[6] N. Ohno and J. D. Wang, "Kinematic Hardening Rules with Critical State of Dynamic Recovery, Part II: Application to experiments of ratcheting behavior", *International Journal of Plasticity,* vol. 9, pp. 391-403, 1993.

[7] M. Abdel-Karim and N. Ohno, "Kinematic hardening model suitable for ratchetting with steady-state", *International Journal of Plasticity,* vol. 16, pp. 225-240, 2000.

[8] G. Kang, "A visco-plastic constitutive model for ratcheting of cyclically stable materials and its finite element implementation", *Mechanics of Materials,* vol. 36, pp. 299-312, 2004.

[9] G. Kang and Q. Kan, "Constitutive modeling for uniaxial time-dependent ratcheting of SS304 stainless steel", *Mechanics of Materials,* vol. 39, pp. 488-499, 2007.

[10] G.-H. Koo and J.-H. Lee, "Investigation of ratcheting characteristics of modified 9Cr–1Mo steel by using the Chaboche constitutive model", *International Journal of Pressure Vessels and Piping,* vol. 84, pp. 284-292, 2007.

[11] M. Yaguchi and Y. Takahashi, "Ratchetting of viscoplastic material with cyclic softening, part 2: application of constitutive models", *International Journal of Plasticity,* vol. 21, pp. 835-860, 2005.

[12] J. Lemaître and J.-L. Chaboche, *Mechanics of solid materials*: Press Syndicate of the University of Cambridge, 1990.

[13] C. O. Frederick and P. J. Armstrong, "A mathematical representation of the multiaxial Bauschinger effect", *Materials at High Temperatures,* vol. 24, pp. 1-26, 2007.

[14] K. Zhang and J. Aktaa, "Ratcheting behavior of Eurofer97 at 550 °C", *Nuclear Materials and Energy,* vol. 15, pp. 97-102, 2018.

[15] A. A. Saad, W. Sun, T. H. Hyde, and D. W. J. Tanner, "Cyclic softening behaviour of a P91 steel under low cycle fatigue at high temperature", *Procedia Engineering,* vol. 10, pp. 1103-1108, 2011.

[16] F. James, *MINUIT Function Minimization and Error Analysis*: CERN, 1994.

[17] J. Aktaa, M. Weick, and M. Walter, High Temperature Creep-Fatigue Structural Design Criteria

for Fusion Components Built from EUROFER 97, Karlsruhe Institute for Technology, FZKA 7309, 2007.

[18] F. Tavassoli, "Eurofer Steel, Development to Full Code Qualification", *Procedia Engineering,* vol. 55, pp. 300-308, 2013.